SPANDIDOS PUBLICATIONS

ONCOLOGY REPORTS 45: 3, 2021

Roles of the SNHG7/microRNA-9-5p/DPP4 ceRNA network in the growth and ^{131}I resistance of thyroid carcinoma cells through PI3K/Akt activation

WANZHI CHEN*, JICHUN YU*, RONG XIE, TAO ZHOU, CHENGFENG XIONG, SHUYONG ZHANG and MEIJUN ZHONG

Department of Thyroid Surgery, The Second Affiliated Hospital of Nanchang University, Nanchang, Jiangxi 330006, P.R. China

Received October 23, 2019; Accepted July 31, 2020

DOI: 10.3892/or.2021.7954

Abstract. Radioactive iodine (RAI, ^{131}I) therapy is the main treatment for thyroid carcinoma (TC). Long noncoding RNA (lncRNA)/microRNA (miR) competing endogenous RNA (ceRNA) networks have aroused great interest for their roles in gene expression. The present study aimed to investigate the effect of lncRNA SNHG7 on the growth and ^{131}I resistance of TC. Differentially expressed lncRNAs in TC and paracancerous tissues were analyzed. The binding of miR-9-5p with small nucleolar RNA host gene 7 (SNHG7) and dipeptidyl-peptidase 4 (DPP4) was identified. Gain- and loss-of-function analyses of SNHG7 and miR-9-5p were performed to determine their effects on the growth and ^{131}I resistance of TC cells. The activity of the PI3K/Akt pathway was evaluated. Consequently, upregulated SNHG7 was revealed in TC tissues and correlated with ^{131}I resistance. Silencing of SNHG7 or overexpressing miR-9-5p inhibited the growth and ^{131}I resistance of TC cells. SNHG7 acted as a ceRNA of miR-9-5p to enhance DPP4 expression. Overexpressed SNHG7 increased DPP4 expression and activated the PI3K/Akt signaling pathway by sponging miR-9-5p. The *in vitro* results were reproduced *in vivo*. In summary, the present study provided evidence that the SNHG7/miR-9-5p/DPP4 ceRNA network could promote the growth and ^{131}I resistance of TC cells via PI3K/Akt activation. The present study may offer novel options for TC treatment.

Correspondence to: Ms. Meijun Zhong, Department of Thyroid Surgery, The Second Affiliated Hospital of Nanchang University, 1 Minde Road, Nanchang, Jiangxi 330006, P.R. China
E-mail: zhongmeijun0523@163.com

*Contributed equally

Key words: thyroid carcinoma, long noncoding RNA small nucleolar RNA host gene 7, ^{131}I resistance, microRNA-9-5p, competing endogenous RNA network

Introduction

Thyroid cancer is the most prevalent endocrine cancer worldwide with rapidly rising morbidity in the past decade owing to the wide use of diagnostic imaging, especially in women (1,2). In 2015, thyroid cancer had the most rapidly increasing incidence rate for women in China (3). Papillary thyroid cancer (PTC) is a major type of thyroid malignancy, accounting for 85% of all thyroid cancer cases (4). Although the mortality rate of PTC is relatively low, with a 5-year survival rate over 95%, the clinical outcomes for severe PTC patients are unfavorable, and the recurrence rate within 3 years was reported to be up to 15.6% in patients who underwent postoperative radioactive iodine (RAI, ^{131}I) treatment (3,5). A primary reason for the unsatisfactory outcome is the failure to respond to ^{131}I ablation treatment after surgical resection caused by the impaired ability of ^{131}I aggregation of thyroid follicular cells (6). Thus, discovering additional molecular mechanisms in ^{131}I resistance and developing potential targets for TC prevention and treatment is of great importance.

Noncoding RNAs, mainly long noncoding RNAs (lncRNAs) and microRNAs (miRs) are well known for their roles in diverse processes through regulation of gene expression (7). Recently, it has been well established that lncRNAs may serve as competing endogenous RNAs (ceRNAs) of miRs by binding to the mRNA response element in miRs, thus regulating gene expression (8). The ceRNA network has been documented to be involved in radioresistance. For instance, lncRNA nuclear-enriched autosomal transcript 1 (NEAT1) has been suggested to act as a ceRNA of miR-101-3p to promote ^{131}I resistance of PTC cells via inactivation of the phosphoinositide 3-kinase/protein kinase B (PI3K/Akt) signaling pathway (5). Among lncRNAs, the small nucleolar RNA host gene (SNHG7) has recently aroused great interest for its tumor promoting roles in several cancer types through binding with miRs (9,10), however its role in PTC remains unclear. miR-9-5p is a well-known tumor inhibitor in multiple cancer types (11,12), including PTC (13). Notably, a previous study suggested that SNHG7 acts as a sponge for miR-9 (14). The present study further identified the target relationship between miR-9-5p and dipeptidyl-peptidase 4 (DPP4). Importantly, upregulation of DPP4 has been

suggested to promote PTC cell growth and metastasis (15). Moreover, downregulation of the PI3K/Akt signaling pathway has been documented to participate in the suppression of PTC growth (16). Overall, this study was designed to identify the interaction among SNHG7, miR-9-5p and DPP4 and to evaluate their roles in the growth and radioresistance of TC cells.

Materials and methods

Ethics statement. The present study was approved and supervised by the Clinical Ethics Committee of the Second Affiliated Hospital of Nanchang University (Nanchang, China). Signed informed consent was obtained from each eligible participant. Animal studies were conducted according to the principles and procedures approved by the Committee on the Ethics of Animal Experiments of the Second Affiliated Hospital of Nanchang University. All experimental procedures were conducted in line with the ethical guidelines for the study of experimental pain in conscious animals.

Clinical sample collection. PTC and paracancerous tissues were collected from 50 PTC patients who were admitted to the Second Affiliated Hospital of Nanchang University from January 2017 to January 2018. Another 50 PTC patients were recruited, and each of them was treated with 10.0 mCi/^{131}I once a month for a total of 6 months. Then, the patients were categorized into responders (n=28) and nonresponders (n=22) to irradiation in accordance with the Response Evaluation Criteria in Solid Tumors version 1.1 (17). We used Arraystar Human lncRNA Microarrray version 2.0 (8660 K; Arraystar) sequencing to analyze the differential expression of lncRNAs between PTC tissues and adjacent tissues. To validate the diagnostic reliability of the lncRNAs in PTC, a receiver operating characteristic (ROC) curve was constructed, and the area under the ROC curve (AUC) of SNHG7 was analyzed.

Microarray analysis. The lncRNAs with differential expression in PTC and paracancerous tissues were predicted and analyzed. The transcriptome data were obtained on an Illumina HiSeq RNA-Seq platform [Illumina HiSeq (Illumina, Inc.), Life Technologies SOLiD (Thermo Fisher Scientific, Inc.), and Roche 454 (Roche Diagnostics)] for 6 PTC tissues and 6 paracancerous tissues. According to The Cancer Genome Atlas (TCGA) (http://ualcan.path.uab.edu/analysis.html) research network, the RNA'Seq PTC dataset contained 60,483 mRNAs that included 7,589 lncRNAs, as described in the NCBI (https://www.ncbi.nlm.nih.gov/) and Ensembl databases (http://www.ensembl.org/). Next, the differential expression of the lncRNAs was assessed using the R language package DESeq (http://www.bioconductor.org/packages/release/bioc/html/limma.html) (18) (criteria set at $P<0.05$ and $|\log_2 FC| >2$). lncRNAs whose expression fold changes were <1 in over 10% of the samples were excluded. Additionally, the expression of each lncRNA was $\log_2$-transformed for the subsequent analysis. Then the online bioinformatics analysis website UALCAN (http://ualcan.path.uab.edu/index.html) (19) was used to predict and screen lncRNA differentially expressed in patients with PTC.

Cell culture and ^{131}I-resistant cell line construction. The TC cell lines TPC-1 (BNCC337912) and B-CPAP (BNCC338685) were purchased from BeNa Culture Collection (Beijing, China). The B-CPAP cell line was identified correctly by STR, and it was not cross-contaminated or misidentified. TPC-1 cells were incubated in 90% Roswell Park Memorial Institute (RPMI)-1640 medium with 10% fetal bovine serum (FBS), while B-CPAP cells were cultured in 90% F-12K medium containing 10% FBS, and they were all incubated at 37˚C with 5% CO_2. All reagents were purchased from Gibco; Thermo Fisher Scientific, Inc. To construct ^{131}I-resistant TPC-1 and ^{131}I-resistant B-CPAP cell lines, the cell medium was mixed with a median lethal dose of ^{131}I. After 24 h of treatment, the cell viability was evaluated using a 3-(4,5-dimethylthiazol-2-yl)-2,5-diphenyltetrazolium bromide (MTT) assay (Promega Corporation) by evaluating the half-maximal inhibitory concentration of ^{131}I (IC_{50}).

Cell transfection. miR-9-5p mimic (50 nM), miR-control, empty vector (pcDNA3.1), overexpression (Oe) SNHG7 vector, Oe-SNHG5 + miR-9-5p, and miR-9-5p + DPP4 were transfected into parent TPC-1 and B-CPAP cells, while Scramble (50 nM), small interfering RNA (siRNA) to SNHG7 (si-SNHG7), miR-9-5p inhibitor (200 nM), si-SNHG7 + miR-9-5p inhibitor and miR-9-5p inhibitor + si-DPP4 (50 nM, Shanghai GenePharma Co., Ltd.) were transfected into res-TPC-1/B-CPAP cells using 2 μl Lipofectamine™ 2000 reagent (Invitrogen; Thermo Fisher Scientific, Inc.). Cells were cultured for 37˚C 24 h, and reverse transcription quantitative polymerase chain reaction (RT-qPCR) was used to verify the transfection efficiency. The sequences were as follows: si-SNHG7-1 sense, 5'-AAUAAUCCGUUUUUACUCCCC-3' and antisense, 5'-GGAGUAAAAACGGAUUAUUUA-3'; si-SNHG7-2 sense, 5'-CGGAUUAUUUAGUCUUCAACA-3' and antisense, 5'-UUGAAGACUAAAUAAUCCGUU-3'; si-SNHG7-3 sense, 5'-GAGACAGUAUCAAGAAAGAUA-3' and antisense, 5'-UCUUUCUUGAUACUGUCUCUU-3'; Scramble sense, 5'-UUCUCCGAACGUGUCACGUTT-3' and antisense, 5'-ACGUGACACGUUCGGAGAATT-3'; si-DPP4, 5'-CCCTATGAAACCGCTGGAAAT-3'; si-DPP4 negative control, 5''TTCTCCGAACGTGTCACGT'3'.

miR-9-5p mimic, 5'-CGAGCTCTGTGTGTGTGTGTG TGTG-3'; miR-9-5p inhibitor: 5'-TTCCGCGGCCGCTAT GGCCGACGTCGACGGGAATGGGGAAAGGGAA-3'.

miR-9-5p mimic negative control, 5'-UUCUCCGAA CGUGUCACGUTT-3'; miR-9-5p inhibitor negative control, 5'-CAGUACUUUUGUGUAGUACAA-3'.

RT-qPCR. Total RNA of cells was extracted according to the instructions of a TRIzol kit (Invitrogen; Thermo Fisher Scientific, Inc.). The purity of total RNA was evaluated using an ultraviolet spectrophotometer, and the absorbance values at 260 nm (A260) and 280 nm (A280) were measured. RNA samples with A260/A280 no less than 1.70 were qualified for subsequent studies. Single-strand cDNA templates were produced by reverse transcription strictly in accordance to the instructions of a Revert Aid First Strand cDNA Synthesis Kit (Thermo Fisher Scientific, Inc.). qRCR was performed using SYBR Premix Ex Taq (Takara Bio, Inc.) on an MX3000P qPCR system (Stratagene; Agilent Technologies, Inc.). Then, PCR amplification was performed with the following conditions: Pre-denaturation at 95˚C for 60 sec, denaturation at 95˚C for

20 sec, annealing at 58˚C for 30 sec and extension at 74˚C for 30 sec. Each experiment was performed in triplicate. The PCR primer sequences and the internal references U6 and glyceraldehyde-3-phosphate dehydrogenase (GAPDH) are presented in Table I. The relative expression was calculated using $2^{-\Delta\Delta Cq}$ (20).

Flow cytometry. Cells ($2x10^6$) were washed with phosphate-buffered saline (PBS) and fixed in Hank's buffered salt solution (product code H1025; Solarbio Life Sciences) (137 mmol/l NaCl, 0.25 mmol/l Na_2HPO_4, 5.4 mmol/l KCl, 0.44 mmol/l KH_2PO_4, 1.0 mmol/l $MgSO_4$, 1.3 mmol/l $CaCl_2$ and 4.2 mmol/l $NaHCO_3$) supplemented with cold 80% ethanol for 30 min. Then, the cells underwent centrifugation at 167.7 x g for 10 min at 4˚C and two PBS washes. Next, the cells were stained with 50 mg/ml propidium iodide [PI; Hangzhou MultiSciences (Lianke) Biotech Co., Ltd.] containing 0.1 mg/ml RNase A and 0.6% NP-40 (Thermo Fisher Scientific, Inc.) at 4˚C under dark conditions for 30 min, subjected to centrifugation at 167.7 x g for 10 min at 4˚C, and washed with PBS. For the apoptosis assay, cells were stained with fluorescein isothiocyanate (FITC)-Annexin V and PI based on the instructions of an Annexin V-FITC/PI kit (BD Biosciences) and then incubated on ice for 15 min without light exposure. Flow cytometry was conducted using a FACSCalibur flow cytometer (BD Biosciences), and FlowJo 10.0.4 software (FlowJo LLC) was used for data analysis. Each procedure was performed 3 times.

5-Ethynyl-2'-deoxyuridine (EdU) labeling assay. An EdU assay was performed to measure DNA synthesis. The inhibition rate of cell proliferation was assessed using a Click-iT EdU Imaging Kit (Thermo Fisher Scientific, Inc.) following a previously reported procedure (21).

MTT assay. An MTT assay was conducted to assess the proliferation of transfected cells. Cells were sorted into 96-well plates at a density of $3x10^3$ cells/well for 3 days, following exposure to 1.0 mCi/well ^{131}I or 0.45 mCi/well ^{131}I. Then, the cells were cultured in 10 μl MTT-8 solution (5 mg/ml, Sigma-Aldrich; Merck KGaA) at 37˚C for 4 h. After 2 h of incubation at 37˚C, 150 μl dimethyl sulfoxide (Sigma-Aldrich; Merck KGaA) was added into each well to dissolve the formazan crystals. Absorbance at 570 nm was read using a microplate reader (Bio-Rad Laboratories, Inc.), and growth curves were generated for each group of cells.

Colony formation assay. Cells were resuspended in RPMI-1640 culture medium in a Luria-Bertani culture plate (cat. no. D0110; Beijing Nobleryder Science and Technology Co., Ltd.) with each plate containing 10 cm medium and 500 cells and cultured in a 37˚C incubator with 5% CO_2 for 2 weeks. Then, the TPC-1 cells were exposed to 1.0 mCi/well ^{131}I, while the B-CPAP cells were exposed to 0.45 mCi/well ^{131}I. Following 20 min of 4% paraformaldehyde fixation at room temperature, the cells were stained with 0.1% crystal violet for 10 min. Then, the plates were air dried, and colonies with at least 50 cells were evaluated under a light microscope (magnification, x100). The relative colony rate was calculated as follows: Relative colony rate=cell colonies in the experimental group/cell colonies in the control group.

Table I. Primer sequences for RT-qPCR.

Primer	Sequence (5'-3')
SNHG7	F: GTGACTTCGCCTGTGATGGA
	R: GGCCTCTATCTGTACCTTTATTC
LINC01977	F: CCCCTTTCCCCAGGGTACTA
	R: CGTTAGACAGCCTCTTGGGG
RP11'363E7.4	F: GGCACTTTTCAGAACATC
	R: TGTCGTGTATCACAGCAT
RP3'483K16.4	F: CCTCGTGCACTCTGGGGTA
	R: GTGGAACTGCTGTGCCAATG
RUNDC3A'AS1	F: CAGTCTCTGTGCGTTGAAGC
	R: GGAGTACACATTGACGGCCA
AC093609.1	F: CGAGTCGGGTTCTGATCCAC
	R: GGATGCTGCTTTCCACCCAT
CTD-2008L17.2	F: AGGGGCCTTCCAGATTAAGG
	R: CGAGTCGGGTTCTGATCCAC
HAGLROS	F: GTCACCCTTAAATACCGCTCT
	R: CTTCCTCCCACACAAATACTCC
UNC5B'AS1	F: CTGGAGGATGAAGGATCGGG
	R: GGCTAGGGGGAAATGTCGG
LINC01354	F: TGCGTTCAGTAAAACGGGCA
	R: TGTGGGAAATGCAGGGTTCT
miR-9-5p	F: CCTGGGAGTATGTCGATCTATTG
	R: TGGTGTCGTGGAGTCG
DPP4	F: AAGTGGCGTGTTCAAGTGTG
	R: GGCTTTGGAGATCTGAGCTG
GADPH	F: CGGACCAATACGACCAA
	R: AGCCACATCGCTCAGACACC

RT-qPCR, reverse transcription quantitative polymerase chain reaction; SNHG7, small nucleolar RNA host gene 7; LINC, long intergenic non-coding; miR, microRNA; DPP4, dipeptidyl-peptidase 4; GADPH, glyceraldehyde-3-phosphate dehydrogenase; F, forward; R, reverse.

Cell cycle assays. Cells ($2x10^6$) were harvested after transfection and then resuspended and fixed in 75% cold ethanol at 4˚C overnight, followed by staining with 100 μl of PI/RNase (BD Biosciences) at 37˚C for 30 min without light exposure. Flow cytometry (Beckman Coulter, Inc.) was used to measure cell populations in the G0/G1, S and G2/M phases. The results were analyzed with cell ModFit LT V5.0 software (Verity Software House, Inc.).

Fluorescence in situ hybridization (FISH). The subcellular localization of SNHG7 was predicted in accordance with the available subcellular localization data at LncATLAS (http://lncatlas.crg.eu/) (22). Next, FISH was conducted to further confirm the subcellular localization of SNHG7 according to the instructions of Ribo™ lncRNA FISH Probe Mix (Green) (Guangzhou RiboBio Co., Ltd.). TPC-1 and B-CPAP cells ($3.5x10^4$ cells/well) were mounted onto slides and fixed in 4% formaldehyde at 4˚C for 10 min. Slides were pretreated with protease K (2 μg/ml; product code P9460;

Solarbio Life Sciences), glycine and acetic anhydride, which was followed by prehybridization at 42˚C for 1 h. Next, the slides were subjected to hybridization using probes against SNHG7 (250 μl; 300 ng/ml) at 42˚C overnight. Then, the slides were stained with PBS-0.1% Tween-diluted 4',6-diamidino-2-phenyl indole (DAPI; product code C0065; Solarbio Life Sciences) at room temperature for 6 min. Images were acquired with a fluorescence microscope (magnification, x1,000) (Eclipse Ti microscope; Nikon Instruments), with five fields randomly selected from each slide.

Fractionation of nuclear/cytoplasmic RNA. The nuclear and cytoplasmic RNA was separated according to the instructions of a PARIS™ Kit (Life Technologies, Inc.; Thermo Fisher Scientific, Inc.). In brief, TPC-1 and B-CPAP cells were resuspended in 500 μl cell fractionation buffer for 5-10 min. Then, the RNA fractions were centrifuged at 500 x g at 4˚C for 5 min for separation. The supernatant (cytoplasmic fraction) was collected into a 2-ml sterile enzyme-free tube and centrifuged, while the pellet (nuclear fraction) was resuspended in 500 μl cell disruption buffer and centrifuged. Next, the fractions were washed with 500 μl 2X lysis/binding solution and centrifuged. Each fraction was then mixed with 500 μl absolute ethanol, transferred into a filter cartridge and rinsed with wash solution. After elution, nuclear and cytoplasmic RNA was collected. SNHG7 expression was detected using RT-qPCR, with U6 as the internal control for nuclear RNA expression and GAPDH for cytoplasmic RNA expression. The primers are presented in Table I.

Western blot analysis. Cells (2x10^6) were lysed in cold radioimmunoprecipitation buffer (product code R0010; Solarbio Life Sciences) supplemented with 1 mM phenylmethylsulfonyl fluoride (product code P8340; Solarbio Life Sciences). The bicinchoninic acid method was used to quantify the extracted protein. Equal volumes of proteins (50 μg) were run on 10% sodium dodecyl sulfate-polyacrylamide gel electrophoresis (Bio-Rad Laboratories, Inc.) and transferred to polyvinylidene fluoride membranes (Amersham Pharmacia; GE Healthcare). After being sealed in 5% skim milk at room temperature for 1 h, western blots were probed with antibodies against Bax (1:1,000; product code ab32503), Bcl-2 (1:1,000; product code ab32124), DPP4 (1:1,000, product code ab114033), Akt (1:500; product code ab8805), p-Akt (1:10,000, product code ab81283), PI3K (1:1,000, product code ab191606), p-PI3K (1:1,000, product code ab182651) and β-actin (1:5,000; product code ab179467) (all purchased from Abcam,) at 4˚C overnight, followed by incubation with the secondary antibody horseradish peroxidase-labeled goat anti-rabbit immunoglobulin G (IgG; 1:2,000; cat. no. A0208, Beyotime Institute of Biotechnology) at 4˚C for 2 h. β-actin was used as a loading control for normalization. Immunoblots were visualized with enhanced chemiluminescence (Amersham Pharmacia; GE Healthcare) and analyzed using ImageJ v1.48u software (National Institutes of Health).

Dual-luciferase reporter assay. starBase (http://starbase.sysu.edu.cn/) (23) and TargetScan (http://www.targetscan.org/vert_72/) (23) were used to predict the target gene of miR-9-5p. The 3'-untranslated region (3'-UTR) fragment of DPP4 mRNA was amplified and cloned into the *Pme*I and *Xba*I sites of the pmirCytomegalovirus vector (pmirCMV; Promega Corparation) to construct DPP4-wild-type (WT) and DPP4-mutant (MUT) plasmids. Similarly, pmirCMV plasmids containing lncRNA SNHG7-WT and lncRNA SNHG7-MUT were also constructed in a similar way. Next, the verified plasmids along with either miR-9-5p mimic or mimic negative control were cotransfected into 293T cells. Every assay was repeated 3 times. Cells were collected 48 h later, and then the luciferase activities were detected using the Dual-CMV Luciferase Assay System (Promega Corpation) and a MicroLumatPlus LB96V luminometer (Berthold Technologies GmbH). The relative luciferase activity was evaluated as the ratio of the firefly luciferase activity to the *Renilla* luciferase activity.

RNA pull-down assay. Cell lysates were treated with RNase-free DNase I (Sigma-Aldrich; Merck KGaA) and cultured with a mixture of 1 μg biotin-labeled miR-9-5p RNA fragments and streptavidin-coated magnetic beads (Sigma-Aldrich; Merck KGaA) in a 4˚C incubator for 3 h. The RNA was isolated from the obtained RNA-protein complexes, and the interacting proteins were subjected to western blot analysis.

Xenograft tumors in nude mice. Female nude mice (N=36; BALB/C nu/nu; ~18-22 g; Beijing Vital River Laboratory Animal Technology Co., Ltd.) had free access to water and food. The mice were raised at 20-22˚C, with humidity 50-60% and a 12-h light/dark cycle. TPC-1 cells transfected with the overexpression plasmid (Oe)-SNHG7, cotransfected with Oe-SNHG7 and miR-9-5p, or transfected with empty vector, and ^{131}I resistant (RAI-res-TPC-1) cells transfected with si-SNHG7 or scramble siRNA were subcutaneously injected into mice at a dose of 3x10^6 cells per mouse. From the day of transplantation to the end of the experiment, the health status and behavior of nude mice were observed every day. Next, the tumor volume (V) was recorded every 3 days and calculated as follows: V (mm^3)=(axb^2)/2, in which 'a' refers to the largest diameter while 'b' refers to the perpendicular diameter. The mice were randomly allocated into 6 groups (6 mice per group) and treated with 2.0 mCi/100 g ^{131}I once the tumor volume reached approximately 70 mm^3. The tumor volume was recorded for up to 35 days. According to the method introduced in the literature (24), the nude mice were euthanized by intraperitoneal injection of pentobarbital (800 mg/kg), and the physical signs of the nude mice were monitored strictly according to the operation. The following experiment was carried out after the complete cessation of the heartbeat of the animals. After subcutaneous injection, all animals bore only one tumor.

Immunohistochemical staining. Sections (5 μm) from xenograft tumors were stained using anti-DPP4 (1:50; product code ab114033; Abcam), anti-p-Akt (1:10,000; ab81283; Abcam) and=anti-Ki67 (1: 200, ab16667; Abcam) at 4˚C overnight and then incubated with anti-IgG secondary antibody (1:1,000; ab6721; Abcam) for 30 min. Staining results were visualized with 3,3-diaminobenzidine (cat. no. DA1010; Solarbio). Five fields were randomly selected and observed under an inverted microscope (Nikon Instruments) at a magnification of x200.

Statistical analysis. Data were analyzed with SPSS 21.0 software (IBM Corp.). Each experiment was performed 3 times. The results are presented as the mean ± standard deviation.

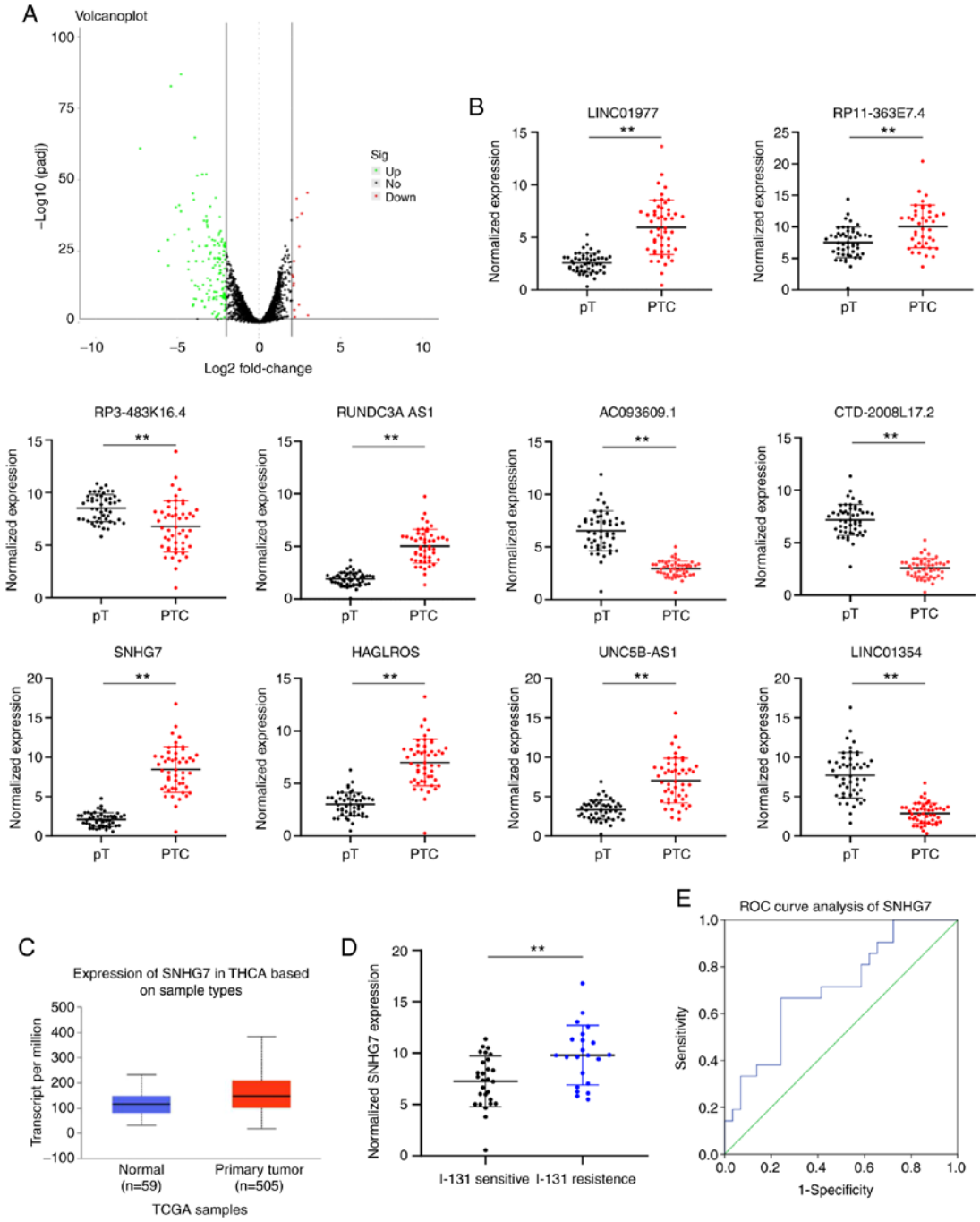

Figure 1. SNHG7 is highly expressed in PTC patients and correlated with ^{131}I resistance. (A) Volcano plot of differentially expressed lncRNAs in PTC and paracancerous tissues, in which the green dots indicate upregulated lncRNAs while the red dots indicate downregulated lncRNAs, and the black dots represent lncRNAs with expression of |log2 FC| <2. (B) Top 10 differentially expressed lncRNAs in PTC and paracancerous tissues identified using RT-qPCR. (C) SNHG7 expression in PTC patients and normal people evaluated via the bioinformatics software UALCAN. (D) The SNHG7 level in responders (^{131}I-sensitive patients) and nonresponders (^{131}I-resistant patients) measured using RT-qPCR. (E) ROC analysis of SNHG7 levels (P<0.05, area under the ROC curve: 0.708; sensitivity: 66.7% and specificity: 75.9%). In B, C and D, data were analyzed using unpaired t-tests. **P<0.01. SNHG7, small nucleolar RNA host gene 7; PTC, thyroid cancer; ^{131}I, radioactive iodine; lncRNA, long noncoding RNA; RT-qPCR, reverse transcription quantitative polymerase chain reaction; ROC, receiver operator characteristic.

Differences in multiple groups were analyzed using one-way or two-way analysis of variance (ANOVA). Tukey's multiple comparison test was utilized for pairwise comparisons after ANOVA. The correlation analysis between each group pair was performed with Pearson's correlation coefficient test. ROC curves were generated, and the area under the ROC curve for lncRNA SNHG7 was analyzed. The P-value was obtained by a two-tailed test, and P<0.05 was considered to indicate a statistically significant difference.

Results

SNHG7 is highly expressed in PTC patients and correlated with ^{131}I resistance. Initially, we analyzed the differentially expressed lncRNAs in PTC and paracancerous tissues, and it was revealed that a total of 169 lncRNAs were differentially expressed. Among them, 145 lncRNAs were upregulated while the remaining 24 were downregulated in PTC tissues (Fig. 1A). To validate the accuracy of the transcriptome data, the top 10

Table II. Characteristics of the top 10 lncRNAs.

Ensemble	Gene	Dysregulation	Fold change	P-value
ENSG00000262772.1	SNHG7	Up	15.19	$1.15x10^{-68}$
ENSG00000260912.1	LINC01977	Up	4.03	$3.75x10^{-27}$
ENSG00000271367.1	RP11'363E7.4	Up	7.86	$5.67x10^{-49}$
ENSG00000233542.1	RP3'483K16.4	Down	11.02	$1.55x10^{-55}$
ENSG00000267750.4	RUNDC3A'AS1	Up	4.38	$5.34x10^{-30}$
ENSG00000230587.1	AC093609.1	Down	4.96	$9.37x10^{-47}$
ENSG00000206129.3	CTD-2008L17.2	Down	6.15	$2.35x10^{-41}$
ENSG00000226363.3	HAGLROS	Up	14.37	$4.78x10^{-24}$
ENSG00000237512.5	UNC5B'AS1	Up	6.06	$1.12x10^{-33}$
ENSG00000231768.1	LINC01354	Down	4.07	$4.87x10^{-19}$

SNHG7, small nucleolar RNA host gene 7; LINC, long intergenic non-coding.

differentially expressed lncRNAs (Table II) were subjected to RT-qPCR in 50 pairs of PTC and paracancerous tissues, and the results revealed the same trend as the transcriptome sequencing results (all P<0.05) (Fig. 1B). Among these lncRNAs, SNHG7 has been demonstrated to increase tumor growth in numerous cancer types (25,26). According to the bioinformation analysis software UALCAN, SNHG7 expression was higher in PTC patients (P<0.05) (Fig. 1C). Moreover, it was determined that high SNHG7 expression was positively associated with ^{131}I resistance in PTC patients (P<0.05) (Fig. 1D). SNHG7 expression revealed diagnostic potential in the prediction of ^{131}I resistance in PTC patients according to the ROC curve and AUC of SNHG7 (area under the ROC curve: 0.708; sensitivity: 66.7% and specificity: 75.9%) (P<0.05) (Fig. 1E).

^{131}I treatment has a poor effect on ^{131}I-resistant PTC cell lines. To further confirm the role of SNHG7 in the ^{131}I resistance and growth of PTC cells, the ^{131}I-resistant cell lines RAI-res-TPC-1 and RAI-res-B-CPAP were constructed by treating the WT PTC cell lines with a median lethal dose of ^{131}I for a total of 8 generations of cells, and the results revealed that the IC_{50} of ^{131}I presented a generation-dependent uptrend. In detail, the IC_{50} of ^{131}I in the first generation of TPC-1 cells was 1.0 mCi/well, while it was 1.9 mCi/well in the 8th generation of RAI-res-TPC-1 cells. The IC_{50} of ^{131}I in the first generation of B-CPAP cells was 0.45 mCi/well, while it was 1.05 mCi/well in the 8th generation of RAI-res-B-CPAP cells (all P<0.05) (Fig. 2A and B). It can be observed from the aforementioned data that the ^{131}I resistance of TPC-1 cells was lower than that of B-CPAP cells. Then, SNHG7 expression was detected in TPC-1 cells and B-CPAP cells and it was revealed that SNHG7 expression in TPC-1 cells was higher than that in B-CPAP cells (Fig. 2C). The MTT assay, flow cytometry and western blot analysis demonstrated that the ^{131}I-resistant cell lines presented higher cell viabilities, less apoptosis (reduced Bax level and increased Bcl-2 level) and higher SNHG7 expression than the parent cells (all P<0.05) (Fig. 2D-H).

Downregulated SNHG7 inhibits the growth and ^{131}I resistance of PTC cells in vitro. To determine the roles of SNHG7 in the growth and ^{131}I resistance of PTC cells, RAI-res-TPC-1 and RAI-res-B-CPAP cells were treated with si-SNHG7 and the parent TPC-1 and B-CPAP cells were treated with Oe-SNHG7 (P<0.05) (Fig. 3A). The results revealed that SNHG7 overexpression promoted the growth of parent PTC cells, demonstrated by fewer cells in the G0/G1 phase and more cells in the S phase (P<0.05) (Fig. 3B-D). Next, PTC-1 and B-CPAP cells were subjected to 1.0 mCi/well or 0.45 mCi/well ^{131}I treatment. Then, it was revealed that silencing of SNHG7 enhanced ^{131}I sensitivity in PTC cells, and overexpressing SNHG7 promoted ^{131}I resistance in parent PTC cells and reduced cell apoptosis after ^{131}I treatment and increased the formation of colonies (P<0.05) (Fig. 3E-G).

SNHG7 is mainly located in the cytoplasm. According to the LncATLAS database, SNHG7 was predicted to mainly localize in the cytoplasm (Fig. 4A). Next, FISH results further demonstrated that SNHG7 was mainly located in the cytoplasm of TPC-1 and B-CPAP cells, since the cytoplasm was stained red by probes targeting SNHG7 and the nucleus was stained blue by DAPI (Fig. 4B). Moreover, total nuclear and cytoplasmic RNA in TPC-1 and B-CPAP cells was separated, and SNHG7 expression in the cytoplasm was higher than that in the nucleus (P<0.05) (Fig. 4C).

SNHG7 functions as a ceRNA of miR-9-5p to upregulate DPP4 expression. The radioresistance-promoting effect of SNHG7 on PTC cells prompted us to determine the underlying mechanism. First, the miRs that could bind to SNHG7 were predicted via starBase. Among them, miR-9-5p has been documented to reverse cell resistance to multiple chemotherapeutics in chronic myelogenous leukemia (27) and to promote the sensitivity of glioma to chemotherapy (28). We hypothesized that SNHG7 may bind to miR-9-5p to reduce the ^{131}I sensitivity of PTC cells. To test this hypothesis, a CMV-based luciferase reporter plasmid containing the binding site of the miR-9-5p mimic or miR-negative control and also SNHG7-WT and SNHG7-MUT were designed in accordance with the starBase prediction, and it was determined that miR-9-5p directly bound to SNHG7 (Fig. 5A-B). This binding relationship was further confirmed by the RNA pull-down assay (all P<0.05) (Fig. 5C). In addition, RT-qPCR revealed a negative correlation between miR-9-5p and SNHG7 expression in 50 PTC patients (Fig. 5D),

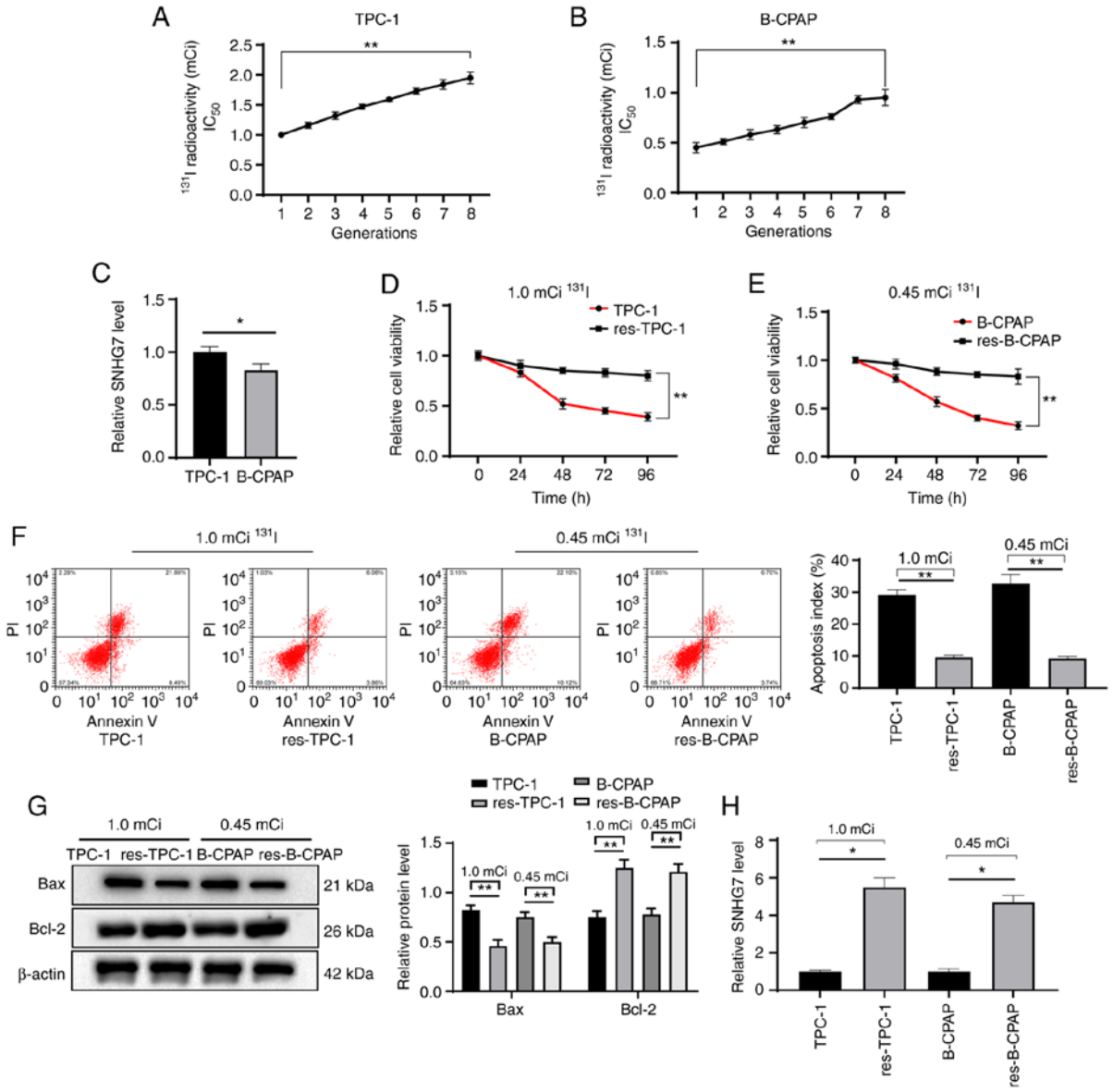

Figure 2. ^{131}I treatment has a poor effect on ^{131}I-resistant PTC cell lines. (A and B) Continuous treatment with the median-lethal dose of ^{131}I in (A) TPC-1 and (B) B-CPAP cell lines. The 1st generation of TPC-1 or B-CPAP was set as the normal cell line, while the 8th generation was the (A) RAI-res-TPC-1 cell line or (B) RAI-res-B-CPAP cell line. (C) SNHG7 expression in TPC-1 and B-CPAP cells determined using RT-qPCR. (D and E) The viability of (D) TPC-1 and RAI-res-TPC-1 cells and (E) B-CPAP and RAI-res-B-CPAP cell lines after ^{131}I treatment assessed with MTT assays. (F and G) Apoptosis of TPC-1, RAI-res-TPC-1, B-CPAP and RAI-res-B-CPAP cell lines treated with ^{131}I assessed with (F) flow cytometry and (G) western blot analysis. (H) SNHG7 expression in TPC-1 and B-CPAP cells determined using RT-qPCR. Replicates=3, data were calculated from one representative experiment and expressed as the means ± standard deviation; in A and B, data were analyzed using one-way ANOVA; in D, E, F, G and H, data were analyzed using two-way ANOVA, and data in C were analyzed by the t-test; *P<0.05, **P<0.01. ^{131}I, radioactive iodine; RAI-res, radioactive iodine (^{131}I)-resistant; PTC, thyroid cancer; MTT, 3-(4,5-dimethylthiazol-2-yl)-2,5-diphenyltetrazolium bromide; RT-qPCR, reverse transcription quantitative polymerase chain reaction; ANOVA, analysis of variance.

and miR-9-5p expression in PTC cells treated with Oe-SNHG7 was further inhibited, while that in cells treated with si-SNHG7 was enhanced (all P<0.05) (Fig. 5E).

Following the result that SNHG7 could target miR-9-5p, we further predicted the target genes of miR-9-5p through starBase and TargetScan. Among the target genes, DPP4 has been documented to increase the growth and metastasis of PTC cells (15). starBase prediction revealed that miR-9-5p could bind to a specific site in the 3'-UTR of DPP4 (P<0.05) (Fig. 5F). Similarly, the dual luciferase reporter assay and RNA pull-down assay were performed, and the results further demonstrated that miR-9-5p could directly bind to DPP4 (all P<0.05) (Fig. 5G and H). The online bioinformatic analysis website UACAN (http://ualcan.path.uab.edu/index.html) (19) indicated that DPP4 expression was higher in PTC patients than in healthy individuals (P<0.05) (Fig. 5I). Moreover, the mRNA expression of DPP4 in PTC patients was negatively associated with miR-9-5p expression and positively associated with SNHG7 (all P<0.05) (Fig. 5J). Oe-SNHG7 (or si-SNHG7) led to enhanced DPP4 levels (or decreased), respectively, and miR-9-5p inhibitor reversed the inhibition of si-SNHG7 on DPP4 expression (all P<0.05) (Fig. 5K). The transfection effect of miR-9-5p inhibitor is presented in Fig. S1.

Overexpressed miR-9-5p reduces SNHG7-induced PTC cell proliferation and ^{131}I resistance. To further identify the

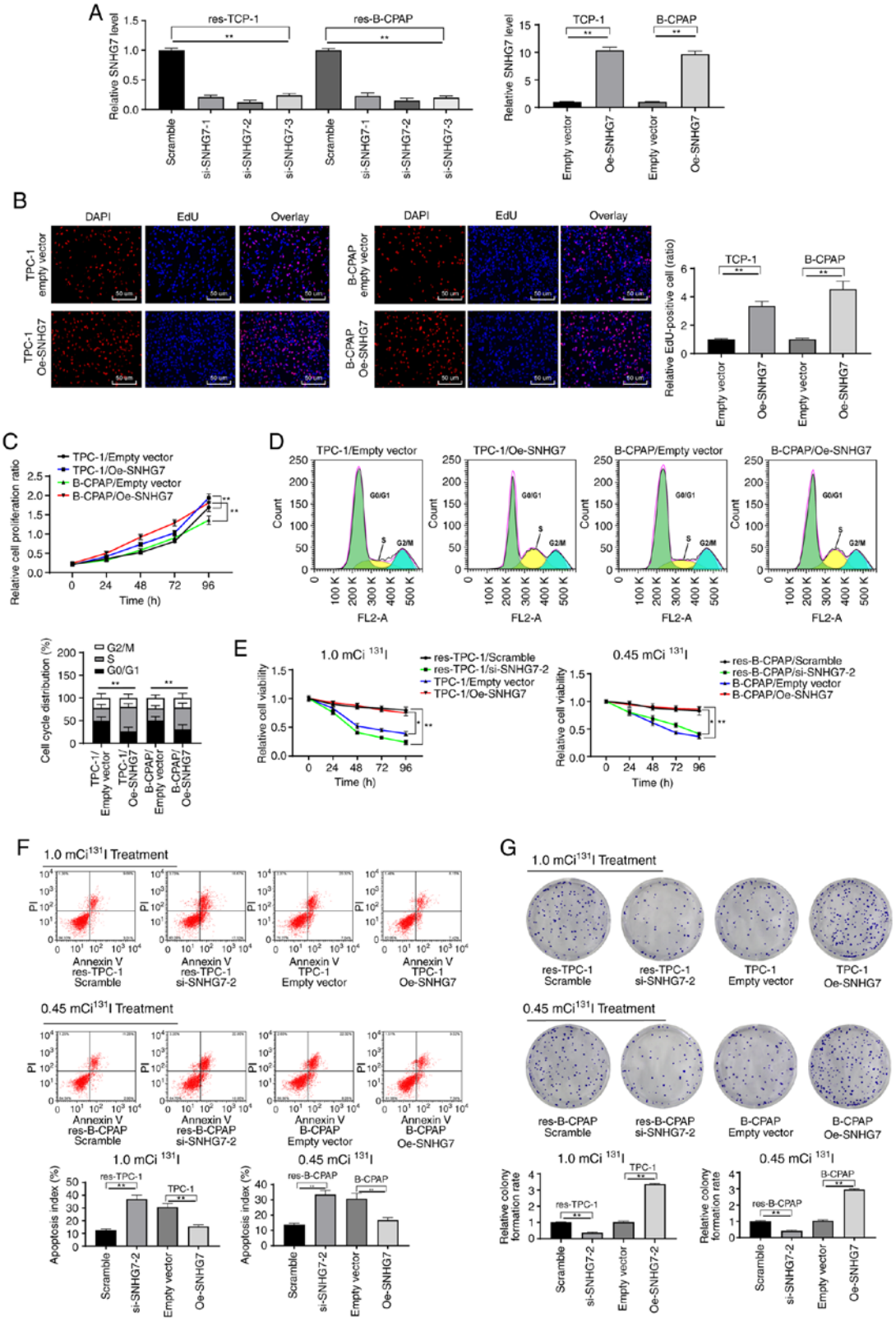

Figure 3. Downregulated SNHG7 inhibits the growth and ^{131}I resistance of PTC cells. Three siRNAs targeting SNHG7 were transfected into RAI-res-TPC-1 and RAI-res-B-CPAP cells (si-SNHG7-1, si-SNHG7-2 and si-SNHG7-3), and an expression vector containing SNHG7 was transfected into parent TPC-1 and B-CPAP cells (Oe-SNHG7 group), with scramble siRNA (mock group) and empty vector (empty vector group) as the negative controls. (A) siRNA and expression vector transfection efficiency validated using RT-qPCR. (B and C) Growth, proliferation and the cell cycle of parent TPC-1 and B-CPAP cells transfected with Oe-SNHG7 detected using (B) EdU, (C) MTT and (D) cell cycle assays. (E) Proliferation of ^{131}I-sensitive and ^{131}I-resistant TPC-1 and B-CPAP cell lines after 96 h of ^{131}I treatment assessed using MTT assays. (F) Apoptosis and (G) colony formation of TPC-1, RAI-res-TPC-1, B-CPAP and RAI-res-B-CPAP cell lines treated with ^{131}I for 12 h measured by flow cytometry. TPC-1 cells were treated with 1.0 mCi ^{131}I, and B-CPA cells were treated with 0.45 mCi ^{131}I. All experiments were repeated three times, and one-way ANOVA was used to determine statistical significance in A, B, F and G; two-way ANOVA was used to determine statistical significance in C, D and E; n=50, *P<0.05, **P<0.01; SNHG7, small nucleolar RNA host gene 7; PTC, thyroid cancer; ^{131}I, radioactive iodine; RAI-res, radioactive iodine (^{131}I)-resistant; Oe, overexpression; si, small interfering; EdU, 5-ethynyl-2'-deoxyuridine; MTT, 3-(4,5-dimethylthiazol-2-yl)-2,5-diphenyltetrazolium bromide; ANOVA, analysis of variance.

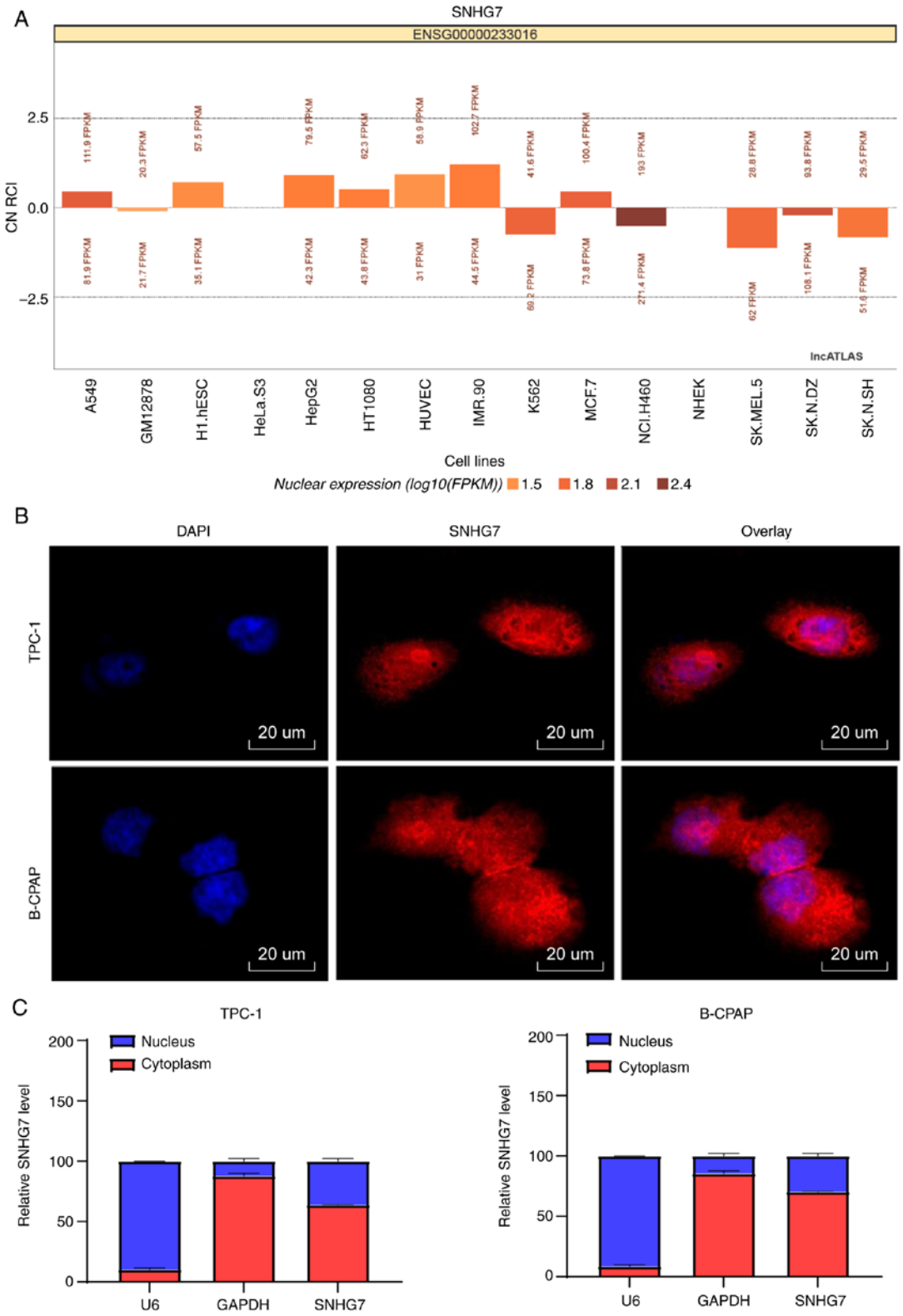

Figure 4. SNHG7 is mainly located in the cytoplasm. (A) Subcellular localization of SNHG7 in the LncATLAS database. (B) Subcellular localization of SNHG7 in TPC-1 and B-CPAP cells validated using FISH. The red fluorescence indicates the cytoplasm stained by probes targeting SNHG7 and the blue fluorescence indicates the nucleus stained by DAPI. (C) Nuclear and cytoplasmic expression of SNHG7 in TPC-1 and B-CPAP cells determined by RT-qPCR. Data are expressed as the mean ± standard deviation, one-way ANOVA and Tukey's multiple comparison test were used for data analysis. SNHG7, small nucleolar RNA host gene 7; DAPI, 4',6-diamidino-2-phenyl indole; RT-qPCR, reverse transcription quantitative polymerase chain reaction; ANOVA, analysis of variance.

roles of miR-9 in the growth and ^{131}I resistance of PTC cells, miR-9-5p mimic was transfected into parental TPC-1 and B-CPAP cells and into RAI-res-TPC-1 and RAI-res-TPC cells, and cotransfected miR-9-5p mimic and Oe-SNHG7 into parental TPC-1 and B-CPAP cells, and the transfection effect was evaluated using RT-qPCR ($P<0.05$) (Fig. 6A). The results revealed that overexpression of miR-9-5p inhibited TPC-1 and B-CPAP cell proliferation and reduced the

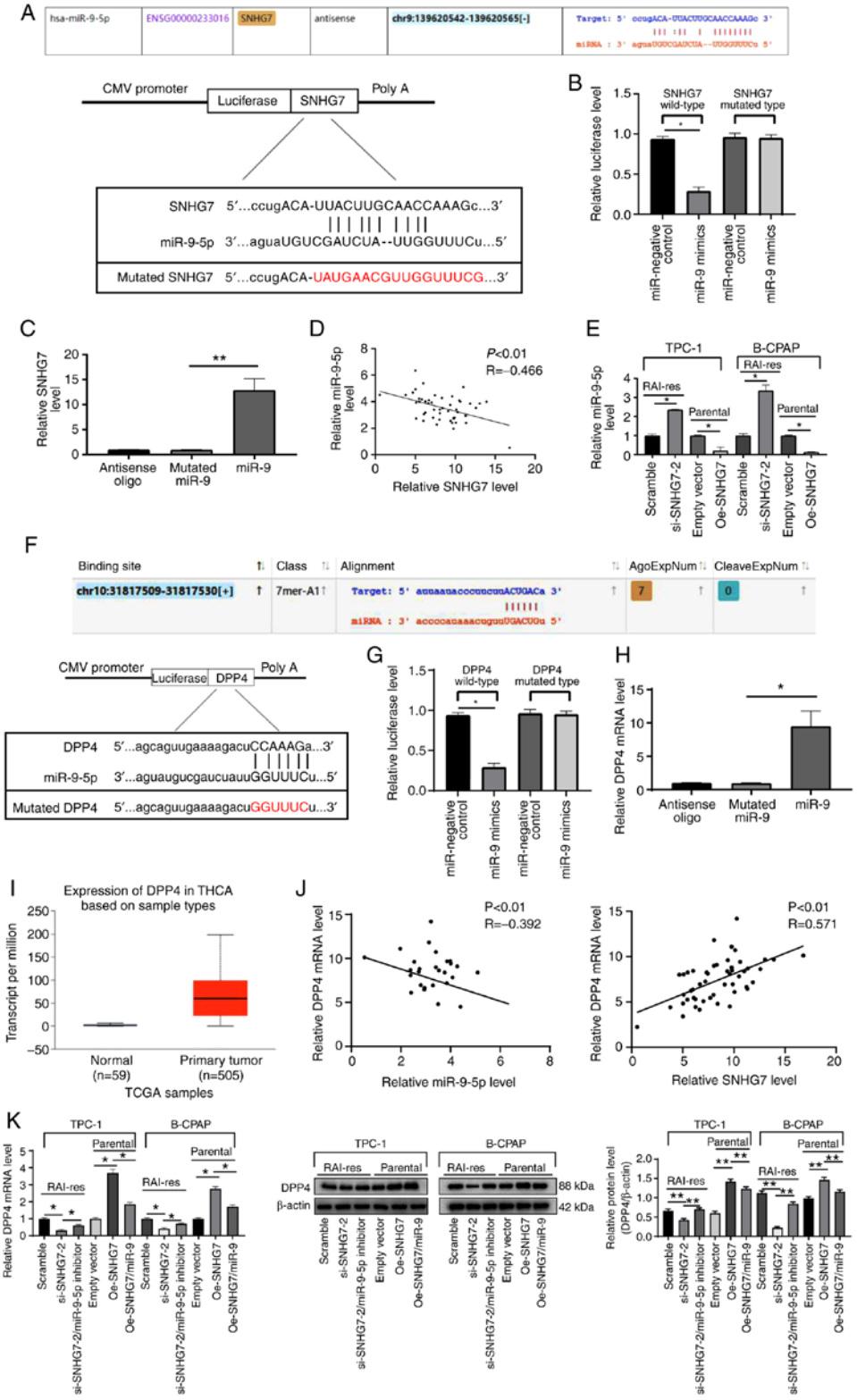

Figure 5. SNHG7 functions as a ceRNA of miR-9-5p to upregulate DPP4 expression. (A) The SNHG7 transcript contains putative miRNA recognition sites complementary to miR-9-5p. (B and C) Target relationship between SNHG7 and miR-9-5p identified using (B) dual luciferase reporter and (C) RNA pull-down assays. (D) Plot analysis of SNHG7 and miR-9-5p expression in 50 PTC patients. (E) miR-9-5p expression after Oe-SNHG7or si-SNHG7 treatment measured using RT-qPCR. (F) Binding relationship between miR-9-5p and DPP4 predicted via starBase. (G and H) Target relationship between miR-9-5p and DPP4 identified using (G) dual-luciferase reporter and (H) RNA pull-down assays. (I) SNHG7 expression in PTC and paracancerous tissues evaluated on UACAN. (J) Plot analysis of miR-9-5p and DPP4 expression in 50 PTC patients. (K) Relative expression of DPP4 mRNA and protein levels after Oe-SNHG7 or si-SNHG7 treatment measured using RT-qPCR and western blot analysis. si-SNHG7-treated RAI-res-TCP-1 and RAI-res-B-CPAP cells were transfected with miR-9-5p inhibitor, while Oe-SNHG7-treated parental TPC-1 and B-CPAP cells were transfected with miR-9-5p mimic. miR-9-5p expression was normalized to U6 expression, while DPP4 mRNA expression was normalized to GAPDH expression. In B, C, E, G, H and K, each experiment was repeated three times, and one-way ANOVA and Tukey's multiple comparison test were used to determine statistical significance, while in D and J, Pearson's correlation coefficient test was utilized; n=50. *P<0.05, **P<0.01. SNHG7, small nucleolar RNA host gene 7; ceRNA, competing endogenous RNA; miRNA, microRNA; DPP4, dipeptidyl-peptidase 4; PTC, thyroid cancer; Oe, overexpression; si, small interfering; RT-qPCR, reverse transcription quantitative polymerase chain reaction; GAPDH, glyceraldehyde-3-phosphate dehydrogenase; ANOVA, analysis of variance; miR-9, microRNA-9-5p.

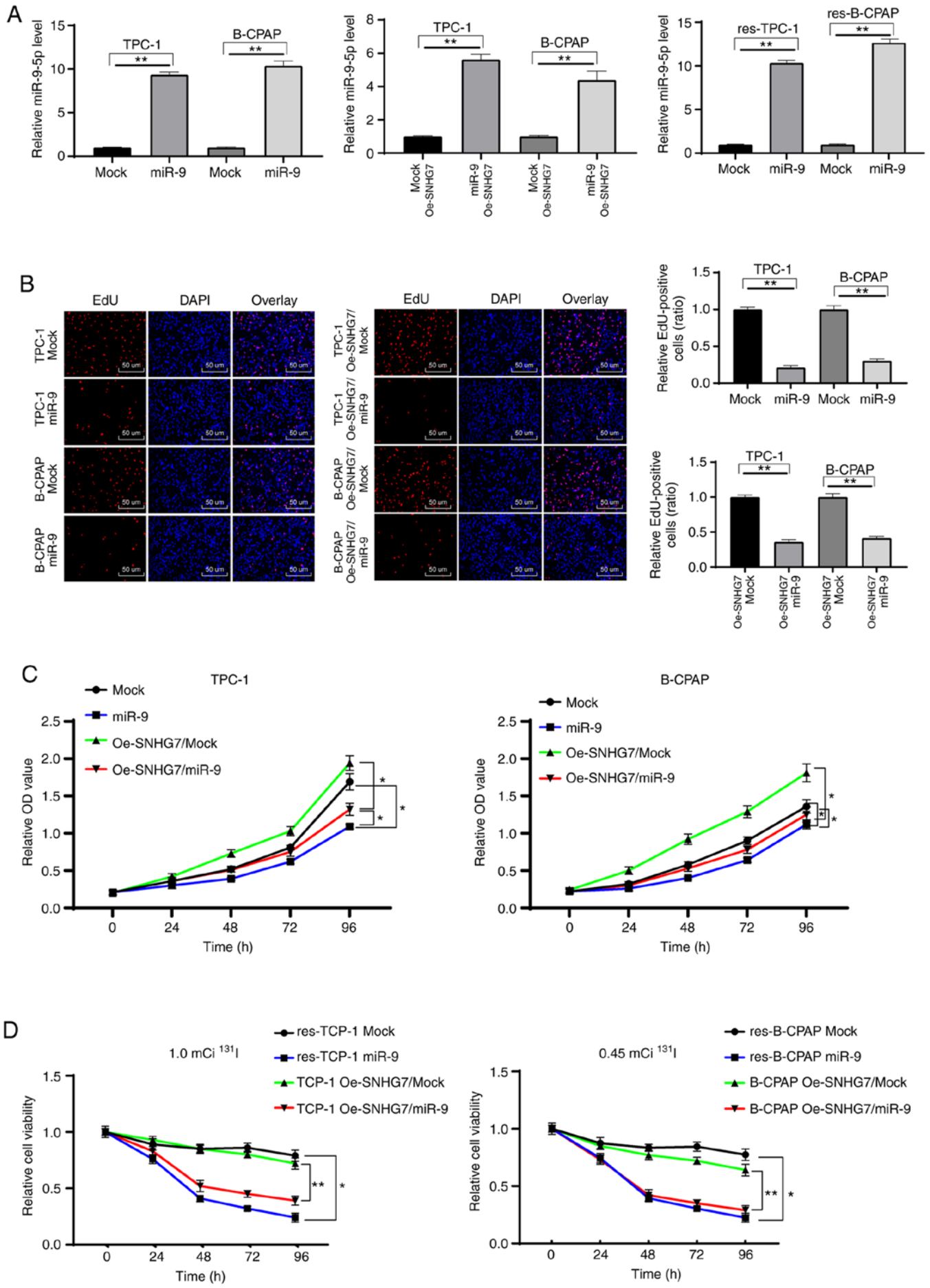

Figure 6. Continued.

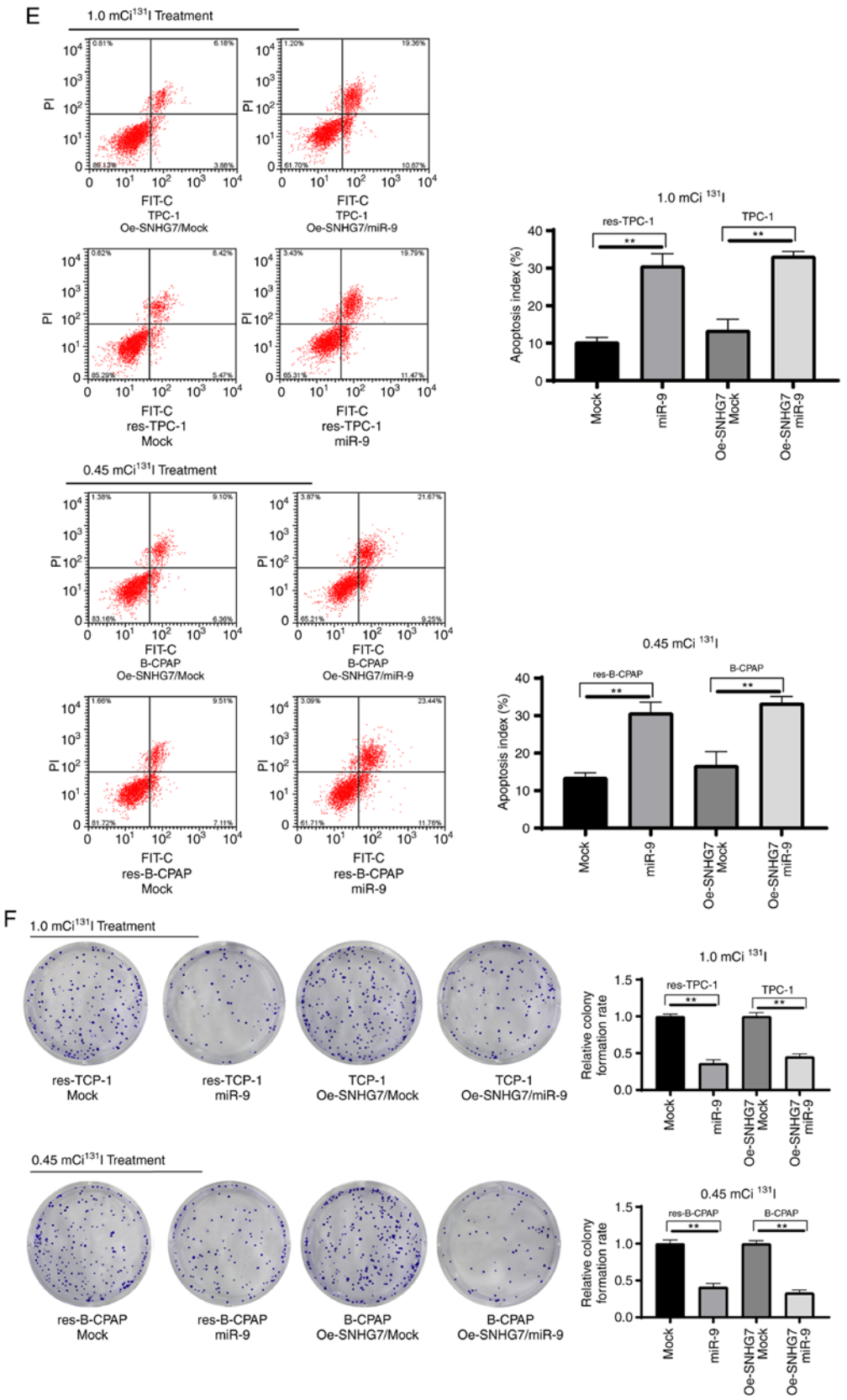

Figure 6. Overexpression of miR-9-5p reduces SNHG7-induced PTC cell proliferation and ^{131}I resistance. Parental TPC-1 and B-CPAP cells, RAI-res-TPC-1 and RAI-res-TPC cells, and Oe-SNHG7-treated parental TPC-1 and B-CPAP cells were transfected with miR-9-5p mimic, and miR-negative control mimic (mock group) was used as the negative control. (A) Transfection efficiency of miR-9-5p evaluated using RT-qPCR. (B and C) The effects of Oe-SNHG7 on parental TPC-1 and B-CPAP cells measured using (B) EdU assay and (C) MTT assay. (D) Proliferation of TPC-1 and B-CPAP cell lines treated for 96 h with ^{131}I (1.0 mCi/well) and ^{131}I (0.45 mCi/well), respectively. (E) Apoptosis and (F) colony formation assays for TPC-1, B-CPAP, RAI-res-TPC-1 and RAI-res-B-CPAP cells subjected to 12 h of ^{131}I treatment measured by flow cytometry. TPC-1 cells were treated with 1.0 mCi ^{131}I, and B-CPAP cells were treated with 0.45 mCi ^{131}I. Replicates=3; one-way ANOVA and Tukey's multiple comparison test were used for data analysis. *P<0.05, **P<0.01. SNHG7, small nucleolar RNA host gene 7; ^{131}I, radioactive iodine; RAI-res, radioactive iodine (^{131}I)-resistant; RT-qPCR, transcription quantitative polymerase chain reaction; Oe, overexpression; EdU, 5-ethynyl-2'-deoxyuridine; MTT, 3-(4,5-dimethylthiazol-2-yl)-2,5-diphenyltetrazolium bromide; ANOVA, analysis of variance; miR-9, microRNA-9-5p.

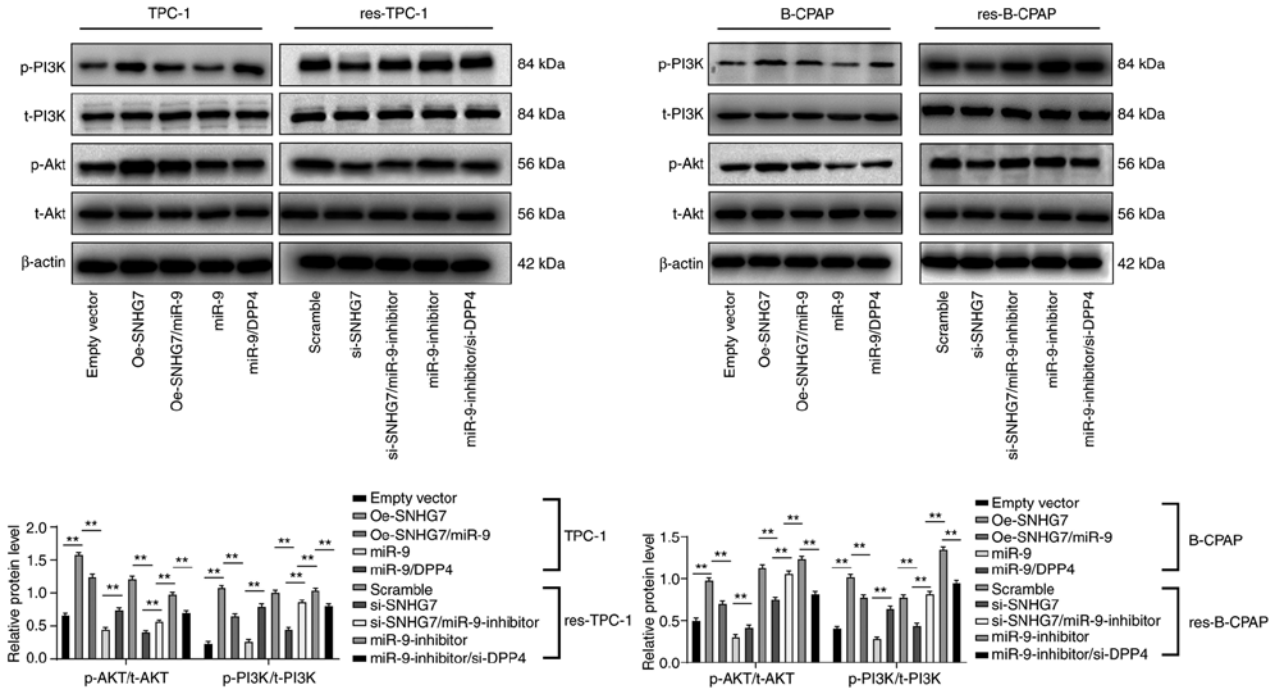

Figure 7. SNHG7 promotes PTC cell resistance and proliferation by activating the PI3K/Akt signaling pathway. TPC-1/B-CPAP cells were transfected with Oe-SNHG7, miR-9-5p mimic, Oe-SNHG7 + miR-9-5p mimic (Oe-SNHG7/miR-9), or miR-9-5p mimic + pcDNA-DPP4 (miR-9/DPP4); while res-TPC-1/B-CPAP cells were transfected with si-SNHG7, si-SNHG7 + miR-9-inhibitor, miR-9-inhibitor, or miR-9-inhibitor + si-DPP4. Scramble siRNA (mock group) and empty vector (empty vector group) served as negative controls. Western blot analysis was performed to determine the activation of the PI3K/Akt signaling pathway in TPC-1 and B-CPAP cells. For PI3K activation, the phosphorylation site was Y-607, while the Akt phosphorylation site was T-308. Replicates=3; two-way ANOVA and Tukey's multiple comparison test were used for data analysis. **P<0.01. SNHG7, small nucleolar RNA host gene 7; siRNA, small interfering RNA; PI3K/Akt, phosphatidyl inositol 3-kinase/protein kinase B; ^{131}I, radioactive iodine; RAI-res, radioactive iodine (^{131}I)-resistant; miR-9, microRNA-9-5p.

Oe-SNHG7-induced ^{131}I resistance of TPC-1 and B-CPAP cells (all P<0.05) (Fig. 6B-F).

SNHG7/miR-9-5p/DPP4 ceRNA network promotes PI3K/Akt activation. Liu *et al* reported that inhibition of the PI3K/Akt signaling pathway induced by silencing SNHG7 can reduce ^{131}I resistance of PTC cells (5). Thus, PI3K/Akt-related protein levels in TPC-1 and B-CPAP cells after SNHG7 interference were assessed. In TPC-1 and B-CPAP cells, compared with the empty vector group, after overexpression of SNHG7, the PI3K/Akt signaling pathway was activated, while overexpression of miR-9-5p reversed these results. Compared with miR-9-5p overexpression alone, overexpression of miR-9-5p and DPP4 activated the PI3K/Akt signaling pathway. In res-TPC-1 and res-B-CPAP cells, the PI3K/Akt signaling pathway was inhibited after SNHG7 expression was inhibited compared with the Scramble group, while the results were reversed after miR-9-5p overexpression. Compared with the inhibition of miR-9-5p expression alone, inhibition of miR-9-5p and DPP4 blocked the PI3K/Akt signaling pathway (all P<0.01) (Fig. 7).

Downregulated SNHG7 inhibits the growth and ^{131}I resistance of PTC cells in vivo. To further investigate the roles of SNHG7 in PTC cell growth *in vivo*, xenograft tumors in nude mice were generated from Oe-SNHG7-treated or miR-9 + Oe-SNHG7-cotreated TPC-1 cells and si-SNHG7-treated RAI-res-TPC-1 cells. No nude mice died in any group during the experiment. The results revealed that Oe-SNHG7 promoted TPC-1 growth *in vivo* and ^{131}I resistance in TPC-1 cells, while si-SNHG7 led to markedly reduced tumor volume and weight (all P<0.05) (Fig. 8A). Moreover, the immunohistochemical results indicated that silencing of SNHG7 led to significantly reduced levels of pAkt, DPP4 and Ki67 (all P<0.05) (Fig. 8B).

Discussion

^{131}I remains a major therapeutic option for differentiated thyroid carcinoma, including PTC, however a great number of PTC patients have reduced iodine uptake thus leading to RAI resistance, which is the main obstacle in PTC treatment and a major cause of poor prognosis (29). lncRNA/miR ceRNA networks have recently gained attention for their roles in regulating gene expression and radiotherapy sensitivity (8,30). The present study was performed to determine the roles of SNHG7 and miR-9-5p in the growth and ^{131}I resistance of PTC cells. The results demonstrated that SNHG7 could serve as a sponge for miR-9-5p to enhance DPP4 expression, and this ceRNA network could induce the growth and ^{131}I resistance of PTC cells via PI3K/Akt activation.

The initial finding of the study was that SNHG7 was aberrantly highly expressed in PTC cells, and overexpressing SNHG7 promoted PTC cell proliferation, while silencing of SNHG7 enhanced the radiosensitivity of ^{131}I-resistant PTC cells. High SNHG7 expression has been revealed in several tumor types, such as nasopharyngeal carcinoma (31), hepatocellular carcinoma (32) and, importantly, thyroid carcinoma (33), with knockdown of SNHG7 leading to inhibited proliferation and metastasis of cancer cells. In addition, downregulation of SNHG7 has been documented to reduce cisplatin resistance

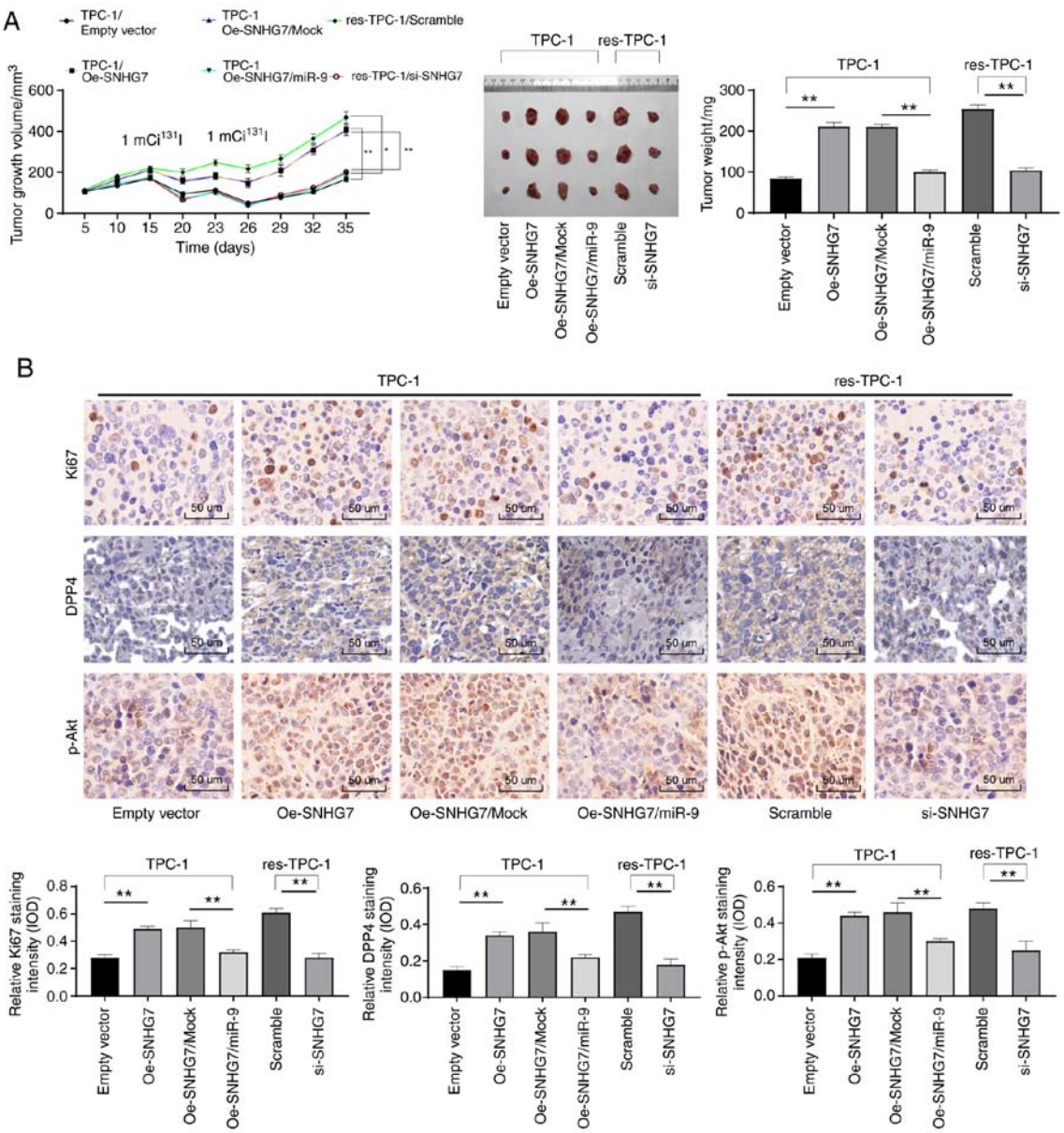

Figure 8. Downregulated SNHG7 inhibits the growth and ^{131}I resistance of PTC cells *in vivo*. TPC-1 cells transfected with Oe-SNHG7 or Oe + miR-9 or scramble siRNA or RAI-res-TPC-1 cells transfected with si-SNHG7 were transfected into BALB/c nude mice (n=6 in each group). From the first day to the 20th day, tumor growth was measured every 5 days, and 20 days later, tumor growth was monitored every 3 days. ^{131}I treatments were conducted with 2.0 mCi/100 g on days 15 and 25 after cell injection. (A) Measurement of tumor volumes and weights in each group of nude mice; tumor sections were collected and stained with anti-DPP4, anti-pAkt and anti-Ki67 antibodies. (B) Relative levels of DPP4, pAkt and Ki67 in each group of tumor cells identified using immunohistochemistry. In A, two-way analysis was used, while in B, one-way analysis was used for data analysis. *P<0.05, **P<0.01. SNHG7, small nucleolar RNA host gene 7; PTC, thyroid cancer; Oe, overexpressed; siRNA, small interfering RNA; ^{131}I, radioactive iodine; RAI-res, radioactive iodine (^{131}I)-resistant; DPP4, dipeptidyl-peptidase 4, pAkt, phosphorylated-protein kinase B; ANOVA, analysis of variance; miR-9, microRNA-9-5p.

in NSCLC cells via PI3K/Akt inhibition (34). Similarly, high expression of SNHG7 has been suggested to be related to an advanced hypopharyngeal cancer stage and higher drug resistance (35). In the present study, it was reported that SNHG7 could also lead to radioresistance in PTC cells.

The promoting role of SNHG7 in PTC cell growth prompted us to further identify the molecules involved in this event. First, we determined the sublocalization of SNHG7 and determined that it was mainly located in the cytoplasm in PTC cells, which provided insights about the potential factors that were involved in SNHG7-induced cell growth. Notably, the present study revealed that SNHG7 could directly bind with miR-9-5p, which was consistent with a previous study (14). In addition, overexpression of miR-9-5p reversed SNHG7-induced growth and radioresistance of PTC cells in the present study. miR-9-5p has been well documented as a tumor inhibitor in several cancer types, such as human gastric cancer (36) and pancreatic cancer (11), and downregulation of miR-9-5p affected by ceRNA networks has been reported to lead to the pathogenesis of numerous cancers (36,37). Notably, miR-9-5p has also been identified as an inhibitor of PTC, whose downregulation led to enhanced proliferation and resistance to apoptosis of PTC cells (13). In addition, miR-9 has been suggested to enhance the sensitivity of glioma to chemotherapy (28) and to markedly improve the therapeutic efficiency of radiotherapy in NSCLC cells (38). Moreover, the present study further

determined that miR-9-5p negatively targeted DPP4, and accordingly, DPP4 expression was positively correlated with SNHG7 expression in PTC patients. DPP4 serves as a tumor biomarker since it is inversely associated with survival in most cancer types (39). Furthermore, it has been documented that upregulation of DPP4 is involved in the growth and development of PTC cells (15). Herein, it was demonstrated that SNHG7 promoted the growth and ^{131}I resistance of PTC cells through the SNHG7/miR-9-5p/DPP4 ceRNA network. In addition, the present study determined that this network promoted PI3K/Akt axis activation. As aforementioned, SNHG7 has been demonstrated to lead to cisplatin resistance through PI3K/Akt activation (34), and a similar trend has also been found in colorectal cancer (40). Moreover, it has also been revealed that overexpression of miR-9-5p inhibits the PI3K/Akt signaling pathway (41). Notably, as aforementioned, PI3K/Akt activation has been implicated in NEAT1-induced ^{131}I resistance in PTC cells (5). Similarly, inhibition of PI3K/Akt signaling has been documented to enhance the radiosensitivity of glioma cells (42). In the present study, it was concluded that the SNHG7/miR-9-5p/DPP4 network could promote the growth and ^{131}I resistance in PTC cells via PI3K/Akt activation.

In summary, the present study demonstrated that SNHG7 could act as a sponge for miR-9-5p to enhance DPP4 expression and further lead to PI3K/Akt activation, thus promoting the growth and radioresistance of PTC cells. However, this research is still at the preclinical stage, and the mechanism of action is not totally elucidated. Thus, more studies in this area are required to validate our findings and to develop clinical strategies or novel therapeutic options for TC treatment.

Acknowledgements

Not applicable.

Funding

The present study was supported by the Natural Science Foundation of China (grant no. 81760320).

Availability of data and materials

All the data generated or analyzed during this study are included in this published article.

Authors' contributions

WC is the guarantor of integrity of the entire study and contributed to the concepts of this study. JY and MZ contributed to the experimental studies and design of this study. RX and TZ contributed to the data and statistical analysis. SZ performed the clinical studies. CX drafted the manuscript and performed the experiments. WC contributed to the critical review of the manuscript for important intellectual content. All authors read and approved the final manuscript.

Ethical approval and consent to participate

The present study was approved and supervised by the Clinical Ethics Committee of the Second Affiliated Hospital of Nanchang University. Signed informed consent was obtained from each eligible participant. Animal studies were conducted according to the principles and procedures approved by the Committee on the Ethics of Animal Experiments of Second Affiliated Hospital of Nanchang University. All experimental procedures were conducted in line with the ethical guidelines for the study of experimental pain in conscious animals.

Patient consent for publication

Not applicable.

Competing interests

The authors declare that they have no competing interests.

References

1. Ding C, Yu H, Shi C, Shi T, Qin H and Cui Y: MiR-let-7e inhibits invasion and magration and regulates HMGB1 expression in thyroid cancer. Biomed Pharmacother 110: 528-536, 2019.
2. Li H, Zhao L, Zhang Z, Zhang H, Ding C and Su Z: Roles of microRNA let-7b in thyroid cancer by regulating HMGA2. Tumour Biol 39: 1010428317719274, 2017.
3. Huang Y, Yu S, Cao S, Yin Y, Hong S, Guan H, Li Y and Xiao H: MicroRNA-222 promotes invasion and metastasis of papillary thyroid cancer through targeting protein phosphatase 2 regulatory subunit b alpha expression. Thyroid 28: 1162-1173, 2018.
4. Gezer E, Selek A, Tarkun I, Canturk Z and Çetinarslan B: Papillary thyroid cancer presenting as a primary renal tumor with multiple pulmonary and bone metastases: A case report. J Med Case Rep 13: 95, 2019.
5. Liu C, Feng Z, Chen T, Lv J, Liu P, Jia L, Zhu J, Chen F, Yang C and Deng Z: Downregulation of NEAT1 reverses the radioactive iodine resistance of thyroid cancer cell via miR-101-3p/FN1/PI3K-AKT signaling pathway. Cell Cycle 18: 167-203, 2019.
6. Xiang C, Zhang ML, Zhao QZ, Xie QP, Yan HC, Yu X, Wang P and Wang Y: lncRNA-SLC6A9-5:2: A potent sensitizer in ^{131}I-resistant thyroid cancer with PARP-1 induction. Oncotarget 8: 22954-22967, 2017.
7. Wan ZY, Song F, Sun Z, Chen YF, Zhang WL, Samartzis D, Ma CJ, Che L, Liu X, Ali MA, *et al*: Aberrantly expressed long noncoding RNAs in human intervertebral disc degeneration: A microarray related study. Arthritis Res Ther 16: 465, 2014.
8. Chen Y, Shen Z, Zhi Y, Zhou H, Zhang K, Wang T, Feng B, Chen Y, Song H, Wang R and Chu X: Long non-coding RNA ROR promotes radioresistance in hepatocelluar carcinoma cells by acting as a ceRNA for microRNA-145 to regulate RAD18 expression. Arch Biochem Biophys 645: 117-125, 2018.
9. Gao YT and Zhou YC: Long non-coding RNA (lncRNA) small nucleolar RNA host gene 7 (SNHG7) promotes breast cancer progression by sponging miRNA-381. Eur Rev Med Pharmacol Sci 23: 6588-6595, 2019.
10. Yao X, Liu C, Liu C, Xi W, Sun S and Gao Z: lncRNA SNHG7 sponges miR-425 to promote proliferation, migration, and invasion of hepatic carcinoma cells via Wnt/β-catenin/EMT signalling pathway. Cell Biochem Funct 37: 525-533, 2019.
11. Wang J, Wang B, Ren H and Chen W: miR-9-5p inhibits pancreatic cancer cell proliferation, invasion and glutamine metabolism by targeting GOT1. Biochem Biophys Res Commun 509: 241-248, 2019.
12. Shi D, Wang H, Ding M, Yang M, Li C, Yang W and Chen L: MicroRNA-26a-5p inhibits proliferation, invasion and metastasis by repressing the expression of Wnt5a in thyroid cancer. Onco Targets Ther 12: 6605-6616, 2019.
13. Guo F, Hou X and Sun Q: MicroRNA-9-5p functions as a tumor suppressor in papillary thyroid cancer via targeting BRAF. Oncol Lett 16: 6815-6821, 2018.
14. Chen Z, Liu Z, Shen L and Jiang H: Long non-coding RNA SNHG7 promotes the fracture repair through negative modulation of miR-9. Am J Transl Res 11: 974-982, 2019.

15. Wang Y, Han J, Lv Y and Zhang G: miR-29a inhibits proliferation, invasion, and migration of papillary thyroid cancer by targeting DPP4. Onco Targets Ther 12: 4225-4233, 2019.
16. Li C, Zhou Y, Cai Y, Shui C, Liu W, Wang X, Jiang J, Zeng D, Gui C and Sun R: Parthenolide inhibits the proliferation of MDA-T32 thyroid cancer cells in vitro and in mouse tumor xenografts and activates autophagy and apoptosis by downregulation of the mammalian target of rapamycin (mTOR)/PI3K/AKT Signaling Pathway. Med Sci Monit 25: 5054-5061, 2019.
17. Eisenhauer EA, Therasse P, Bogaerts J, Schwartz LH, Sargent D, Ford R, Dancey J, Arbuck S, Gwyther S, Mooney M, *et al*: New response evaluation criteria in solid tumours: Revised RECIST guideline (version 1.1). Eur J Cancer 45: 228-247, 2009.
18. Ritchie ME, Phipson B, Wu D, Hu Y, Law CW, Shi W and Smyth GK: limma powers differential expression analyses for RNA-sequencing and microarray studies. Nucleic Acids Res 43: e47, 2015.
19. Chandrashekar DS, Bashel B, Balasubramanya SA, Creighton CJ, Ponce-Rodriguez I, Chakravarthi BV and Varambally S: UALCAN: A portal for facilitating tumor subgroup gene expression and survival analyses. Neoplasia 19: 649-658, 2017.
20. Livak KJ and Schmittgen TD: Analysis of relative gene expression data using real-time quantitative PCR and the 2(-Delta Delta C(T)) method. Methods 25: 402-408, 2001.
21. Chehrehasa F, Meedeniya AC, Dwyer P, Abrahamsen G and Mackay-Sim A: EdU, a new thymidine analogue for labelling proliferating cells in the nervous system. J Neurosci Methods 177: 122-130, 2009.
22. Mas-Ponte D, Carlevaro-Fita J, Palumbo E, Hermoso Pulido T, Guigo R and Johnson R: LncATLAS database for subcellular localization of long noncoding RNAs. RNA 23: 1080-1087, 2017.
23. Agarwal V, Bell GW, Nam JW and Bartel DP: Predicting effective microRNA target sites in mammalian mRNAs. Elife 4: e05005, 2015.
24. Zatroch KK, Knight CG, Reimer JN and Pang DS: Refinement of intraperitoneal injection of sodium pentobarbital for euthanasia in laboratory rats (Rattus Norvegicus). BMC Vet Res 13: 60, 2017.
25. Deng Y, Zhao F, Zhang Z, Sun F and Wang M: Long noncoding RNA SNHG7 promotes the tumor growth and epithelial-to-mesenchymal transition via regulation of miR-34a signals in osteosarcoma. Cancer Biother Radiopharm 33: 365-372, 2018.
26. Shan Y, Ma J, Pan Y, Hu J, Liu B and Jia L: lncRNA SNHG7 sponges miR-216b to promote proliferation and liver metastasis of colorectal cancer through upregulating GALNT1. Cell Death Dis 9: 722, 2018.
27. Li Y, Zhao L, Li N, Miao Y, Zhou H and Jia L: miR-9 regulates the multidrug resistance of chronic myelogenous leukemia by targeting ABCB1. Oncol Rep 37: 2193-2200, 2017.
28. Li Q, Chang Y, Mu L and Song Y: MicroRNA-9 enhances chemotherapy sensitivity of glioma to TMZ by suppressing TOPO II via the NF-κB signaling pathway. Oncol Lett 17: 4819-4826, 2019.
29. Amit M, Na'ara S, Francis D, Matanis W, Zolotov S, Eisenhaber B, Eisenhaber F, Weiler Sagie M, Malkin L, Billan S, *et al*: Post-translational regulation of radioactive iodine therapy response in thyroid cancer. J Natl Cancer Inst: Dec 1, 2017 (Epub ahead of print). doi: 10.1093/jnci/djx092.
30. Hu X, Ding D, Zhang J and Cui J: Knockdown of lncRNA HOTAIR sensitizes breast cancer cells to ionizing radiation through activating miR-218. Biosci Rep 39: BSR20181038, 2019.
31. Wang L, Xu T, Cui X, Han M, Zhou LH, Wei ZX, Xu ZJ and Jiang Y: Downregulation of lncRNA SNHG7 inhibits proliferation and invasion of nasopharyngeal carcinoma cells through repressing ROCK1. Eur Rev Med Pharmacol Sci 23: 6186-6193, 2019.
32. Sun BZ, Ji DG, Feng ZX and Wang Y: Long noncoding RNA SNHG7 represses the expression of RBM5 to strengthen metastasis of hepatocellular carcinoma. Eur Rev Med Pharmacol Sci 23: 5699-5704, 2019.
33. Wang YH, Huo BL, Li C, Ma G and Cao W: Knockdown of long noncoding RNA SNHG7 inhibits the proliferation and promotes apoptosis of thyroid cancer cells by downregulating BDNF. Eur Rev Med Pharmacol Sci 23: 4815-4821, 2019.
34. Chen K, Abuduwufuer A, Zhang H, Luo L, Suotesiyali M and Zou Y: SNHG7 mediates cisplatin-resistance in non-small cell lung cancer by activating PI3K/AKT pathway. Eur Rev Med Pharmacol Sci 23: 6935-6943, 2019.
35. Wu P, Tang Y, Fang X, Xie C, Zeng J, Wang W and Zhao S: Metformin suppresses hypopharyngeal cancer growth by epigenetically silencing long Non-coding RNA SNHG7 in FaDu Cells. Front Pharmacol 10: 143, 2019.
36. Fan Y, Shi Y, Lin Z, Huang X, Li J, Huang W, Shen D, Zhuang G and Liu W: miR-9-5p suppresses malignant biological behaviors of human gastric cancer cells by negative regulation of TNFAIP8L3. Dig Dis Sci 64: 2823-2829, 2019.
37. Xie CH, Cao YM, Huang Y, Shi QW, Guo JH, Fan ZW, Li JG, Chen BW and Wu BY: Long non-coding RNA TUG1 contributes to tumorigenesis of human osteosarcoma by sponging miR-9-5p and regulating POU2F1 expression. Tumour Biol 37: 15031-15041, 2016.
38. Wei W, Dong Z, Gao H, Zhang YY, Shao LH, Jin LL, Lv YH, Zhao G, Shen YN and Jin SZ: MicroRNA-9 enhanced radiosensitivity and its mechanism of DNA methylation in non-small cell lung cancer. Gene 710: 178-185, 2019.
39. Javidroozi M, Zucker S and Chen WT: Plasma seprase and DPP4 levels as markers of disease and prognosis in cancer. Dis Markers 32: 309-320, 2012.
40. Li Y, Zeng C, Hu J, Pan Y, Shan Y, Liu B and Jia L: Long non-coding RNA-SNHG7 acts as a target of miR-34a to increase GALNT7 level and regulate PI3K/Akt/mTOR pathway in colorectal cancer progression. J Hematol Oncol 11: 89, 2018.
41. Yi J and Gao ZF: MicroRNA-9-5p promotes angiogenesis but inhibits apoptosis and inflammation of high glucose-induced injury in human umbilical vascular endothelial cells by targeting CXCR4. Int J Biol Macromol 130: 1-9, 2019.
42. Gwak HS, Kim TH, Jo GH, Kim YJ, Kwak HJ, Kim JH, Yin J, Yoo H, Lee SH and Park JB: Silencing of microRNA-21 confers radio-sensitivity through inhibition of the PI3K/AKT pathway and enhancing autophagy in malignant glioma cell lines. PLoS One 7: e47449, 2012.